Faraday Discussions

Cite this: *Faraday Discuss.*, 2014, **168**, 533

PAPER

Wavelength resolved UV photodesorption and photochemistry of CO_2 ice

J.-H. Fillion,*[a] E. C. Fayolle,[b] X. Michaut,[a] M. Doronin,[a] L. Philippe,[a] J. Rakovsky,[a] C. Romanzin,[c] N. Champion,[d] K. I. Öberg,[e] H. Linnartz[b] and M. Bertin[a]

Received 11th December 2013, Accepted 6th January 2014
DOI: 10.1039/c3fd00129f

Over the last four years we have illustrated the potential of a novel wavelength-dependent approach in determining molecular processes at work in the photodesorption of interstellar ice analogs. This method, utilizing the unique beam characteristics of the vacuum UV beamline DESIRS at the French synchrotron facility SOLEIL, has revealed an efficient *indirect* desorption mechanism that scales with the electronic excitations in molecular solids. This process, known as DIET – desorption induced by electronic transition – occurs efficiently in ices composed of very volatile species (CO, N_2), for which photochemical processes can be neglected. In the present study, we investigate the photodesorption energy dependence of pure and pre-irradiated CO_2 ices at 10–40 K and between 7 and 14 eV. The photodesorption from pure CO_2 is limited to photon energies above 10.5 eV and is clearly initiated by CO_2 excitation and by the contribution of dissociative and recombination channels. The photodesorption from "pre-irradiated" ices is shown to present an efficient additional desorption pathway below 10 eV, dominating the desorption depending on the UV-processing history of the ice film. This effect is identified as an *indirect* DIET process mediated by photoproduced CO, observed for the first time in the case of less volatile species. The results presented here pinpoint the importance of the interconnection between photodesorption and photochemical processes in interstellar ices driven by UV photons having different energies.

Introduction

In recent years it has become clear that the non-thermal desorption of molecules from ice-covered dust grains plays an important role in determining the balance

[a]*Laboratoire de Physique Moléculaire pour l'Atmosphère et l'Astrophysique (LPMAA), CNRS UMR 7092, UPMC Univ. Paris 6, F-75252 Paris, France*
[b]*Sackler Laboratory for Astrophysics, Leiden Observatory, Leiden University, P. O. Box 9513, NL-2300 RA Leiden, The Netherlands*
[c]*Laboratoire de Chimie Physique (LCP), CNRS UMR 8000, Univ. Paris Sud, F-91400 Orsay, France*
[d]*LERMA, UMR 8112 du CNRS et Observatoire de Paris, 4 place J. Jansen, 92195 Meudon Cedex, France*
[e]*Harvard-Smithsonian Center for Astrophysics, 60 Garden Street, Cambridge, MA 02138, USA*

between gas phase and solid state species in the interstellar medium (ISM). Non-thermal desorption, for example, explains the astronomically observed gas phase abundances of species at temperatures well below their accretion value. Among the non-thermal desorption pathways, photon-stimulated desorption (PSD) appears to be a dominant mechanism, particularly in protoplanetary disks, but this process also is considered to be relevant in other regions where ices are exposed to UV photons.[1–4] Photodesorption rates, for instance, are needed to predict the position of snowlines in protoplanetary environments.[1,5] Quantifying and constraining photodesorption processes in sufficient detail is therefore a prerequisite for incorporation into astrochemical networks. Equally important is the thorough understanding of the underlying molecular processes.

The focus of this paper is carbon dioxide; CO_2 is one of the most abundant molecules present in interstellar ice after H_2O and CO, with abundances relative to solid H_2O varying from ~15 to 40% along many lines of sight.[6–8] In the gas phase, typical abundances relative to H_2 of about $\sim 10^{-7}$ have been reported in warm and cold gas towards low and high mass protostars, where it acts as an important tracer of the chemical and physical history.[9,10] The observed solid state abundances in the ISM are 100-fold higher than in the gas phase and cannot be reproduced by gas phase chemical models, which is the reason why it is generally accepted that CO_2 forms in the solid state. In protostellar environments, CO_2 can be found in H_2O-rich or CO-rich ices, and it has also been observed as pure ice most likely originating from thermal processing and segregation of ice mixture components.[11,12] CO_2 has been observed in the upper layers of protoplanetary disks in the gas phase and in the condensed phase,[13] the latter resulting most likely from recondensation of upper layers and from incorporation of protostellar ice material.

The photodesorption of CO_2 ice has been the subject of several experimental studies over the last five years. Öberg *et al.* investigated thin ice photodesorption by combining infrared reflection spectroscopy (RAIRS) and mass spectrometry (MS) to monitor ice depletion with irradiation time, and explored the influence of various physical parameters on the desorption efficiency.[14] They found a major effect following the photodissociation of CO_2 into CO and O and subsequent recombination to form energetic CO_2, resulting in thickness and temperature dependent photodesorption rates. Yuan and Yates[15,16] investigated isotopic effects in the photodesorption and photochemical decomposition of $^{12}CO_2/^{13}CO_2$ ice at 75 K, and concluded that these originate from differences in electronic energy transfer efficiencies from excited CO_2 molecules to the ice matrix. Combining quartz microbalance techniques and mass spectrometry, Bahr and Baragiola[17] reported very large desorption yields for CO, O_2 and O from highly photoprocessed CO_2 ices at 40–60 K. Very recently, high desorption rates following radiation damage at high photon fluence combined with thermally activated desorption have been observed for crystalline CO_2 ice (75 K).[18] Besides these approaches based on discharge lamps, pump-probe laser-based experiments were performed by Kinugawa *et al.*[19] at 7.9 eV, yielding a state selective detection of $O(^3P)$ and CO ($v = 0, 1$) photofragments in the gas phase, arising from the photodissociation of CO_2 trapped in amorphous CO_2:H_2O samples at 90 K. Wavelength dependent photodesorption studies of CO_2 have not been reported to date.

UV-induced photo-processes in interstellar ice analogs have been simulated using different light sources. The most commonly applied source is the

microwave discharge H_2 flow lamp, which provides high UV photon fluxes (typically 10^{13}–10^{15} photons cm^{-2} s^{-1}). Such "broad-band" photon-sources are believed to be well-suited to simulate UV interstellar fields, because they provide atomic hydrogen Lyman alpha emission at 10.2 eV (121.6 nm), which is quasi-ubiquitous in space, together with (depending on operating conditions) continuous emission at lower energies between 7 and 9 eV.[20] For decades such lamps have been used to study photochemical processes in generally thick (thousands of monolayers) ice mixtures, applying infrared and more recently also optical spectroscopy (*e.g.* ref. 21). Hydrogen discharge lamps were also the first systems widely used to derive absolute photodesoption rates of various and generally thinner (a few ML up to a few tens of ML thick) interstellar ice analogs, such as solid H_2O, CO, or CO_2.[14,22–25] The method applied in these studies is that the time dependent decrease in absolute surface density is recorded using infrared spectroscopy, eventually supported by simultaneous mass recording of the ejected species. With a known UV photon flux it is then possible to calculate the desorption rate.

In recent years the development of a new undulator-based VUV beamline (DESIRS) on the 2.75 GeV storage ring SOLEIL (Saint-Aubin, France) has provided an optimal flux-to-resolution solution, presenting the opportunity to investigate photo-processes with a continuously tunable monochromatic source combining (among other properties) high spectral purity and high photon fluxes.[26] In parallel to this development, the "Surface Processes & ICES" (SPICES, UPMC, Paris) set-up has been designed with the aim of coupling it with the DESIRS beamline, in order to initiate wavelength-dependent vacuum UV photodesorption studies. The approach relies on photon-stimulated desorption (PSD) experiments, in which atomic/molecular species are ejected from an ice film into the gas phase upon monochromatic vacuum UV (VUV) irradiation. The calibrated detection through mass spectroscopy as a function of the incident photon energy provides a unique wavelength-dependent signature of the ice photodesorption, reflected by a so-called PSD spectrum. The investigation of the VUV photodesorption of CO ice films at 18 K in the 7–14 eV energy range has benchmarked a series of new experimental studies supported by this approach.[27] Firstly, this has provided the absolute wavelength-dependent photodesorption rates needed in astrochemical models to interpret different radiation fields. Secondly, it has proven to be extremely powerful for revealing the underlying molecular processes. Our PSD spectra of pure ices composed of light volatiles species such as CO and N_2 have provided the first experimental proof of a desorption induced by electronic transition (DIET) mechanism, which dominates most of the desorption events taking place between 7 and 14 eV.[27,28] As an illustration, Fig. 1a displays the PSD spectrum recorded for VUV irradiated pure CO and N_2 ice samples. The spectra clearly reveal two vibrationally-resolved electronic transitions, identified as CO $A^1\Pi(\nu') - X^1\sum(\nu'' = 0)$ and N_2 $b\,^1\Pi_u(\nu') - X\,^1\sum_g(\nu'' = 0)$, which reflect the absorption properties of solid CO (below 10 eV) and solid N_2 (above 12 eV), respectively. Systematic investigations of these typical fingerprints in (isotopically labeled) ices layered samples led to the conclusion that DIET takes place in the near-surface region of the ice, involving at most the upper three molecular layers of the ice film.[29] By further investigating N_2:CO-mixed (and -layered) samples, the desorption from a mixed (or layered) film was found to be radically different than

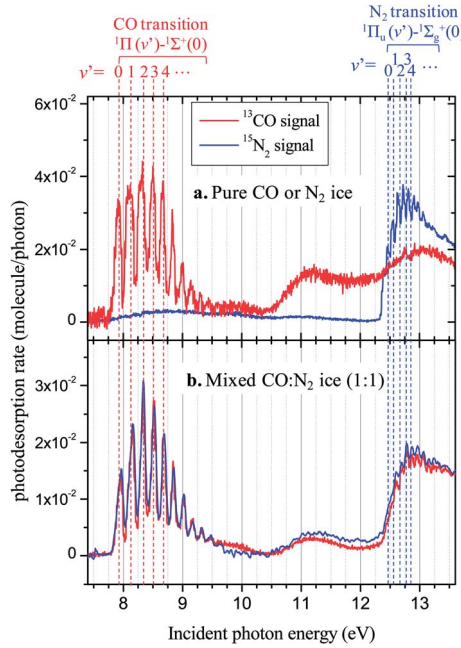

Fig. 1 Photon-stimulated desorption (PSD) spectra of (a) ^{13}CO from a pure ^{13}CO ice and N_2 from a pure $^{15}N_2$ ice, and of (b) $^{15}N_2$ and ^{13}CO from a condensed (1 : 1) mixture of ^{13}CO and $^{15}N_2$. The spectra have been acquired from 30 ML-thick ices, deposited on HOPG, and kept at 15 K. The electronic transitions in condensed CO (in red) and condensed N_2 (in blue), responsible for the desorption are indicated. The spectra in the lower panel show evidence that the photodesorption rates of both CO and N_2 from the mixture are identical, and are the combination of the photo-excitation of each pure component.[30]

that observed for a pure ice sample. In particular, Bertin *et al.*[30] showed that the efficient desorption of one specific chemical component in a binary ice can be observed for wavelengths where the corresponding pure ice does not desorb upon VUV radiation.[30] This is linked to the concept of indirect desorption illustrated in Fig. 1b, which compares the CO and N_2 desorption from a N_2:CO (1 : 1) ice mixture. It is worth noting that the PSD spectra of the two species from the ice mixture are identical in Fig. 1b. The N_2 desorption below 10 eV is due to CO $A^1\Pi$ – $X^1\sum$ excitation, and in the same way the CO desorption above 12 eV is a direct consequence of N_2 $b^1\Pi_u$ – $X^1\sum_g$ excitation. These PSD spectra illustrate the indirect nature of the DIET process, since the prompt relaxation of the excited molecular states can be transferred to neighboring molecules and up to weakly bound surface species independent of their chemical nature.[30] Such an *indirect adsorbate-mediated* process has also been suggested to play a role in the desorption of water from layered ices of water and benzene irradiated by UV laser pulses.[31] The indirect nature of the desorption process reinforces the critical importance of the photon energy distribution of the light source in order to understand how the chemical composition and internal organization of the ice surface affect the photodesorption rates from a complex icy sample.

Since most stable molecules possess electronic states accessible in VUV, it is of particular interest to investigate possible indirect DIET desorption mechanisms

for heavier and more strongly bound species. Moreover, previous studies have focused on molecules that are very stable upon VUV excitation, *i.e.* species that do not efficiently photodissociate. Especially for polyatomic molecules, energetic radiation can cause fragmentation and it is not fully clear how this affects or competes with other surface processes, such as photodesorption. This is the topic of the present study, in which VUV irradiation of CO_2 ice films is used to investigate the energy dependence of the photodesorption and its interconnection with photochemistry. The wavelength dependent approach, as described above, is used to investigate the primary processes at play to explain the desorption of the parent molecule and its photoproducts. We will show here that pure, as-grown CO_2 ices and photoprocessed ices behave differently. For a pure CO_2 ice sample, most of the intact CO_2 and photoproduced CO molecules are ejected in the gas phase for incident photon energies higher than 10.5 eV. For photoprocessed ices, the presence of CO as a photochemical product can explain the enhancement of CO_2 desorption below 10 eV due to an indirect desorption effect.

Experimental section

The photodesorption studies were performed in the SPICES set-up of UPMC (Paris, France). This device is an ultrahigh vacuum system with a base pressure of $\sim 1 \times 10^{-10}$ Torr. Molecular ices were grown either onto a polycrystalline gold or a highly oriented pyrolitic graphite (HOPG) substrate, mounted on the cold tip of a closed-cycle helium cryostat. Its temperature can be controlled in the 10–300 K range with 0.5 K precision, using a resistive heating system.

$^{13}CO_2$ (Eurisotop, 99.18% ^{13}C) ice samples were prepared *in situ* and introduced at low flow speed into the chamber *via* a dosing tube, positioned $\sim$2 mm in front of the substrate. This geometry allows the condensation of $^{13}CO_2$ ices onto the cold surface without a substantial increase in the background pressure of the set-up. The thickness of the resulting ice is expressed in monolayers (ML), which corresponds to the surface density of a compact molecular layer on a flat surface (1 ML $\approx 10^{15}$ molecules cm^{-2}). This thickness can be controlled by varying the exposure time during the ice growth. The experimental conditions allow for satisfactory ice thickness reproducibility, with a precision better than 1 ML.

The ices were irradiated across the 7 to 14 eV range using the monochromatized output of the undulator-based beamline DESIRS of the SOLEIL synchrotron facility.[26] The SPICES set-up was directly connected to the beamline end *via* a differential pumping stage, thus preventing any cut-off of high energy photons by a coupling window. The photon energy can be fixed or scanned over a wide range. A narrow bandwidth of typically 40 meV was selected by the 6.65 m normal incidence monochromator that is implemented on the beamline. A rare gas filter in the beamline suppressed the higher harmonics of the undulator that can be transmitted in higher diffraction orders of the grating. Calibrated photodiodes installed on the beamline were used to precisely determine the photon flux as a function of the photon energy. In our configuration, the applied energy-dependent photon flux varied from 0.8 to 2.6×10^{13} photons s^{-1} cm^{-2} over the 7–14 eV range. This monochromatized mode for the beamline was used for either irradiating the ices at a fixed energy and at a given dose, or scanning the incident photon energy to record energy-resolved photodesorption rates.

Energy-resolved photodesorption spectra were recorded as follows. The incident photon energy was scanned from 7 to 14 eV with 25 meV steps. Simultaneously, photodesorbed species were detected in the gas phase using a Quadrupole Mass Spectrometer (QMS). The gas phase mass signal was thus monitored as a function of the incident energy, resulting in a PSD spectrum. The mass signal can be converted into an absolute number of desorbing molecules. This calibration has been done for CO ices by correlating the depletion of the condensed molecules, probed by infrared spectroscopy, with the mass signal of ejected molecules during irradiation.[27] In the case of $^{13}CO_2$, this procedure needs special attention, as chemistry can occur during the irradiation; consequently, correlating the condensed $^{13}CO_2$ infrared signature to gas phase ejected $^{13}CO_2$ is not straightforward. Instead, the $^{13}CO_2$ gas phase signal has been calibrated using the pre-existing CO calibration, corrected by different electron-impact ionization cross sections in the QMS, as taken from Freund *et al.*[32] In addition, we have verified that the apparatus function of our QMS for the two masses, 28 amu (CO) and 45 amu ($^{13}CO_2$), is the same to within a few percent. In this way, using the measured energy-dependent photon flux as a function of the photon energy, we can derive the absolute photodesorption rate, in desorbed molecules per incident photon, for a given photon energy. It is important to note that this data treatment procedure does not significantly alter the shape of the spectra, since all the structures in the calibrated PSD spectra are already clearly observed in the raw mass signal data. More details on the data quantification procedure can be found in Fayolle *et al.*[28]

The $^{13}CO_2$ ices were also probed after deposition, and during or after irradiation, by means of RAIRS. In our case, this method mainly allows for the identification of the condensed phase composition, and in particular for the observation of photochemistry during irradiation at fixed energy. Fine quantification of the condensed phase composition was performed using the temperature programmed desorption (TPD) method; the sample was warmed up at a constant heating rate (3 K min^{-1}), and the thermally desorbed species were measured as a function of the temperature by mass spectrometry. Unlike RAIRS, this method is sensitive to very low amounts of molecules (less than 0.1 ML), and can differentiate species as a function of their binding energy to the ice, *i.e.* whether they are bulk or surface-located. Each irradiated sample was probed using TPD in order to quantify the eventual photoproducts formed upon UV irradiation. Obviously, a TPD experiment destroys the ice and is only performed after the photoprocessing has fully taken place.

In both PSD and TPD, the gas phase mass signal of desorbing ^{13}CO was corrected from the fragmentation of intact $^{13}CO_2$ in the QMS. The ^{13}CO signal originating from $^{13}CO_2$ fragmentation was systematically subtracted from the overall ^{13}CO signal, in order to probe only the desorbing ^{13}CO molecules.

Results

Fig. 2a shows the photodesorption rates measured between 7 and 14 eV from pure $^{13}CO_2$ ice at 10 K and 40 K. The quadrupole mass spectrometer can simultaneously detect $^{13}CO_2$ and ^{13}CO species (in the gas phase). As explained in the experimental section, absolute photodesorption rates are obtained (i) by calibrating the gas phase mass signal to the absolute amount of ejected molecules,

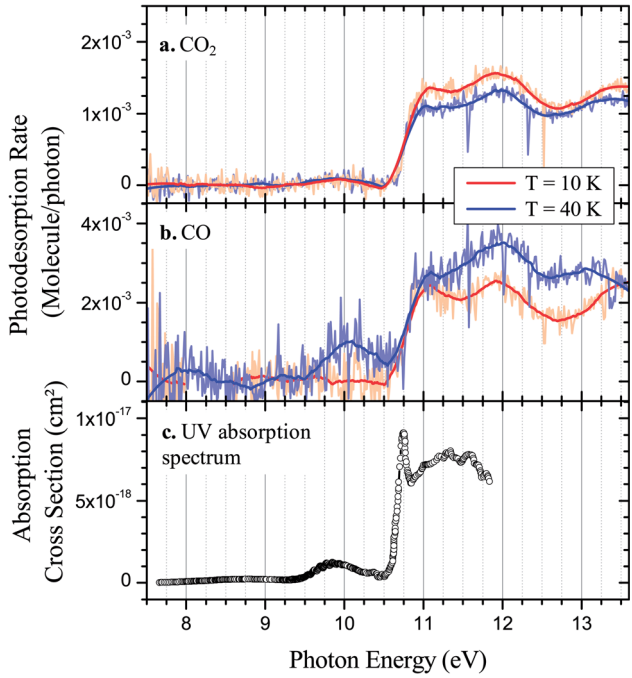

Fig. 2 PSD spectra of $^{13}CO_2$ (a) and ^{13}CO (b) from 10 ML-thick $^{13}CO_2$ ices. The ices were deposited on a polycrystalline Au substrate and kept at 10 K and 40 K. Panel (c) shows, for comparison, the absorption spectra of solid CO_2, as measured by Monahan and Walker.[33] The spectrum has been calibrated in the absorption cross section using the data from Mason *et al.*[34] and Cruz-Diaz *et al.*[35]

and (ii) by taking into account the variations in measured photon flux with photon energy. The PSD spectra reveal a very strong energy dependence of the $^{13}CO_2$ and ^{13}CO photodesorption rates. Below about 10.5 eV, the photodesorption rate for both species is essentially zero, but a sudden increase is found around this value, with a more or less continuous and efficient desorption at higher energies. Very similar and small variations are observed for the $^{13}CO_2$ and ^{13}CO species above 11 eV, with photodesorption rates varying between 1×10^{-3} to 3×10^{-3} molecules photon^{-1}.

The PSD spectra are compared to the absorption spectrum of solid $^{12}CO_2$ at 53 K from Monahan and Walker,[33] as shown in Fig. 2c, in which the absorption is measured in natural logarithmic absorbance ($\ln(I_0/I)$, in which I_0 is the incident intensity and I is the transmitted intensity, for different ice thicknesses. There is no absorption spectrum available for $^{13}CO_2$, but only small differences between the two isotopologues are expected. These values have been normalized for a given thickness, and absolute cross sections were calibrated using the quantitative data of Mason *et al.*[34] and Cruz-Diaz *et al.*[35] in the 9–10.5 eV energy range. In the lower energy range, $E < 10.5$ eV, the absorption spectrum is associated with valence state excitations and comprises a lower lying diffuse absorption band centered around 8.6 eV, overlapping with a second more intense absorption band centered around 9.8 eV with an irregular vibrational structure, as reported in detail by Mason *et al.*[34] These transitions are commonly assigned to the optically

forbidden (but vibronically allowed) transitions $^1\Delta_u - {}^1\sum_g^+$ and $^1\Pi_g - {}^1\sum_g^+$ for the 8.6 eV and 9.8 eV band, respectively.[33,36] Recent high-level *ab initio* calculations of isolated CO_2 molecules indicate that this energy region is very complex due to multiple degeneracies of six valence states linked through a network of couplings due to the Renner–Teller effect, and conical intersections either at linearity in the Franck–Condon region or at bent geometries.[37] According to the gas-phase spectrum interpretation, the intensity distribution can be explained by non-vertical transitions originating from Herzberg–Teller effects in the transition dipole moments. The first band involves electronic transitions towards two bent electronic components, $2^1A'/{}^1A''$ ($1\ ^1\Delta_u$ at linearity), and an additional weak transition towards the $2^1A''$ ($^1\sum_u^-$ at linearity) excited state. At higher energy, the second band is assigned to a transition to the linear $3^1A'/3^1A''$ ($1\ ^1\Pi_g$) states, and is more intense due to "intensity borrowing", most probably from the allowed $1\ ^1\sum_u^+$ Rydberg states lying at higher energy.[38] The absorption oscillator strength of this second band at 9.8 eV is even more enhanced in the solid phase.[33] A very weak photodesorption signal is visible around 10 eV in the PSD spectra of $^{13}CO_2$ and ^{13}CO (Fig. 2a and b).

The onset around 10.5 eV observed in the photodesorption rates correlates with the enhancement by almost one order of magnitude of the absorption cross sections in solid CO_2 above 10.5 eV. In the higher energy domain ($E > 10.5$ eV), the strong absorption is associated with dipole allowed transitions from the ground state towards $(np\sigma_u)^1\sum_u^+$ and $(np\pi_u)^1\Pi_u$ Rydberg states (with $n \geq 3$), and possible contributions of other series (s, d and f Rydberg series) converging to the first ionization potential, as observed in the gas phase.[39,40] The intense absorption peak observed at 10.7 eV (Fig. 2c) has been associated with the first dipole allowed electronic transition $(3p\sigma_u)^1\Sigma_u^+ - {}^1\Sigma_g^+$.[36] Apart from this first peak, which is not seen in any of the photodesorption spectra, the photodesorption efficiency follows the photoabsorption continuum above 11 eV, although the comparison cannot be extended beyond 11.75 eV, since absorption spectra of solid CO_2 are lacking above this value. The broad band observed at 11.6 eV in the CO_2 photodesorption spectrum may be associated with the excitation of the $(3p\pi_u)^1\Pi_u$ state, as suggested by electron energy loss spectroscopy.[41] Finally, another band observed at 13 eV matches the ionization energy of solid CO_2.[42]

In the gas phase, CO_2 is known to photodissociate upon energetic VUV irradiation. Experiments show that excitation of the diffuse absorption bands ($^1\Delta_u$ and $^1\Pi_g$) leads to atomic oxygen production with quantum yields close to unity. Consequently, the photodissociation of CO_2 into $O(^1D)$ + $CO(^1\Sigma^+)$ and $O(^3P)$ + $CO(^1\Sigma^+)$ dominates the photolysis below 10.5 eV.[43–45] Between 10.5 eV and 14.5 eV, new photodissociation channels open, providing additional pathways to produce efficiently excited atoms $O(^1S)$ and excited CO ($a^3\Pi$) molecules.[46,47] The formation of excited $O(^1S)$ atoms resulting from reactive processes following UV excitation of CO ($CO^* + O \rightarrow CO_2^* \rightarrow CO + O^*$) have been identified in Ar cryogenic matrices experiments.[48,49] In the solid phase, however, the photodecomposition efficiency is expected to be strongly reduced with respect to the gas phase. This is due either to possible reactive collisions between O and CO fragments on the surface or within the ice matrix, forming CO_2, or to the electronic quenching of the electronic excited states producing vibrationally hot CO_2 molecules.[16] In addition, the reaction between excited and non-excited photofragments such as CO ($a^3\Pi$) + CO ($X^1\Sigma$) $\rightarrow$ CO_2 + C, cannot be excluded and may also decrease the CO_2 photolysis

efficiency compared to the gas phase.[50] Nevertheless, excitation of CO_2 is expected to lead to partial photofragmentation into CO and O on a very short time scale (10^{-15} s). As shown in Fig. 2, the shape of the PSD spectra of CO and CO_2 recorded in the low temperature (10 K) experiments are very similar, showing a steep onset at 10.5 eV. It should be noted that the CO photodesorption rates are higher than those of CO_2, indicating that, despite their common origin, the desorption processes follow different underlying mechanisms. Photodesorption rates that are higher for CO than for CO_2 have also been reported by others.[14,17,18] This behavior is consistent with CO desorption arising from direct CO_2 photodissociation, kicking fragments into the gas phase. Oxygen atoms are indeed also detected simultaneously by mass spectrometry and give similar PSD spectra. No quantitative analysis of the oxygen desorption rates for the atoms has been performed. This is not possible as the fractionation of several heavier O-bearing species in the QMS contributes strongly to the overall signal at 16 amu.

Fig. 2a and b compare the CO_2 and CO PSD spectra obtained at 10 and 40 K. The 40 K CO_2 PSD spectrum does not show any desorption around 10 eV. A weak CO_2 desorption might be present at 10 K, but the desorption rates ($\sim 9 \times 10^{-5}$ molecules photon^{-1}) are close to the noise level and are highly uncertain. By contrast, a temperature effect is observed in the 40 K PSD spectrum of CO, which desorbs at around 10 eV, in correlation with the 9.8 eV absorption band of CO_2 (Fig. 2c). A temperature effect is even more clearly observed between 11 and 14 eV. As the temperature increases from 10 to 40 K, the CO_2 desorption rates decrease quasi-uniformly by 10% (Fig. 2a). Interestingly, an opposite behavior is simultaneously observed for CO; here the desorption rates are higher at 40 K (Fig. 2b). This effect can be explained by differences in the binding energies of the two species. As will be discussed in more detail in the next section, the adsorption energy of CO on CO_2 ice is about 90 meV, which corresponds to an onset for CO desorption at $\sim$25 K, peaking at 40 K. Therefore, at 40 K, we expect that the CO desorbs just after its formation in the condensed phase. On the contrary, CO_2 is more strongly bound to the CO_2-rich surface, with a binding energy of 230 meV,[51] and its thermal desorption is negligible on the experimental time scale. The enhancement of the CO desorption at 40 K can thus be explained by the contribution of thermally activated desorption of CO molecules from the top ice layers. Contribution from the CO molecules in the underlying surface layers is also possible. The observation that the desorption of CO molecules is accompanied by a lowering of the CO_2 photodesorption rates is fully consistent with the picture in which the photoproduced CO molecules – lost upon thermal desorption – are in fact those contributing to the desorption of CO_2. This mechanism will be explained in detail in the discussion section.

In order to further investigate the possible role of CO in the photodesorption process, we irradiated a $^{13}CO_2$ ice film at higher photon fluences but only for a few selected energies. Typically, 10 ML thick $^{13}CO_2$ ice films at 10 K were pre-irradiated with a 7×10^{16} photon dose. This irradiation mode is well-suited to separately excite different regions of the CO_2 ice absorption spectrum. Irradiation with photons at 7.2 eV, 8.7 eV, 9.8 eV, and 11 eV was performed with a narrow 40 meV bandwidth resulting from the monochromator. The pre-irradiation at 7.2 eV can be used as a blank experiment, since the CO_2 ice film does not absorb at this energy. After each pre-irradiation sequence, the sample was again investigated in a similar way to that described above by recording the PSD spectrum. The results are shown in Fig 3.

After pre-irradiation at 8.7 eV, 9.8 eV, and more markedly at 11 eV, the CO desorption rates increase and a strong desorption pattern with a new structure appears in the 7–10 eV energy range (Fig. 3b). This structure originates from the CO $A^1\Pi(\nu') - X^1\Sigma(\nu'' = 0)$ electronic transition, as shown in Fig. 1, that has been studied in much detail in previous works.[27,29,52] This feature is a clear signature of an ongoing DIET process, indicating the presence of high concentrations of CO in the upper layers of the ice film. Moreover, this was confirmed by complementary TPD measurements. Fig. 4 displays the ^{13}CO desorption peak corresponding to thermal desorption from the ice film between 30 and 75 K. A comparison can be made with the thermal desorption of 1 ML of CO deposited on CO_2 ice, *i.e.* recorded without photon irradiation. As expected, no significant CO signal, *i.e.*, clearly discernible from the background noise, was detected from the ice film after irradiation at 7.2 eV, for which the CO_2 ice is transparent. For all other energies, the TPD spectra can be integrated to estimate the CO ice concentration within the ice film. From the comparison with the desorption of 1 ML CO from CO_2, the CO surface concentration (*i.e.* in the top layers of the ice that contribute to the desorption process) was determined to amount to roughly 4%, 20% and 45% after pre-irradiation at 8.7 eV, 9.8 eV and 11 eV, respectively. The CO ice concentration increases with increasing photon energy due to the

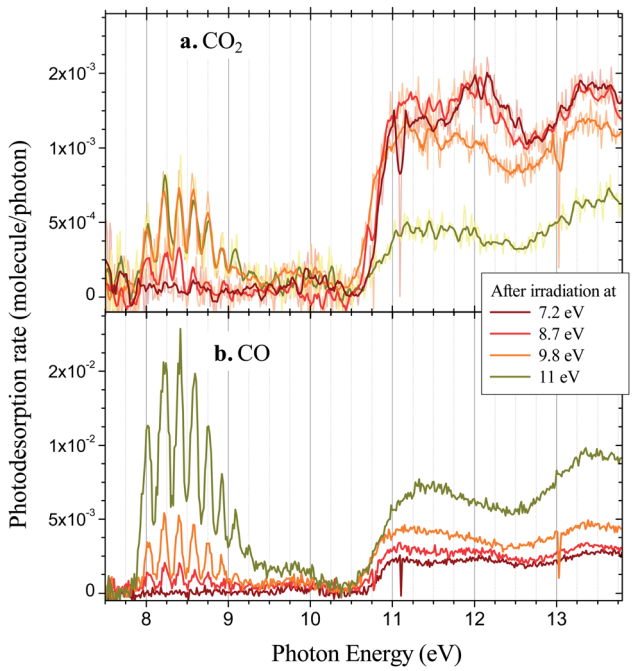

Fig. 3 PSD spectra of $^{13}CO_2$ (a) and ^{13}CO (b) from 10 ML-thick $^{13}CO_2$ ices, pre-irradiated at fixed energies (7.2, 8.7, 9.8 and 11 eV). The ices were deposited on a polycrystalline Au substrate and kept at 10 K. The pre-irradiation was realized with a fluence of 7×10^{16} photons for each energy. The structure appearing in the low energy part of the spectra is associated with the excitation of CO molecules formed in the ice during the pre-irradiation. The prevalence of this structure at higher pre-irradiation energies is linked to the greater quantity of CO formed in the solid.

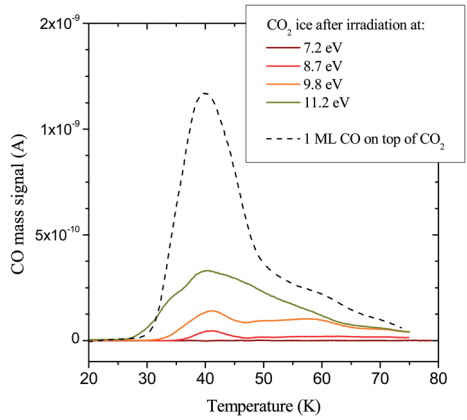

Fig. 4 Temperature programmed desorption (TPD) curves of ^{13}CO from 10 ML-thick ^{13}CO ices, deposited on polycrystalline Au kept at 10 K, and pre-irradiated with a fluence of 7×10^{16} photons at 7.2, 8.7, 9.8 and 11 eV. The TPD curve of 1 ML of ^{13}CO deposited at 10 K on 10 ML of $^{13}CO_2$ is presented for comparison (dashed line). The TPD was carried out with a temperature ramp of 3 K min^{-1}. The shapes of the TPD curves for the pre-irradiated ices are very similar to that of surface CO on top of CO_2, which allows the conclusion that these molecules most probably originate from the top layers of the pre-irradiated ices. The integrals of the TPD signals give the amount of CO formed during the pre-irradiation located on the (sub)surface of the ice.

increasing values of the CO_2 absorption cross sections for these four selected energies (Fig. 2c).

The CO_2 PSD spectra after pre-irradiation are shown in Fig. 3a. The CO_2 desorption is significantly affected by the presence of CO on the surface of the ice film. At first, new desorption structures are observed between 8–9 eV, with relatively high CO_2 photodesorption rates. This effect is particularly noticeable since in this energy region only an extremely weak CO_2 desorption could be observed from fresh CO_2 films. The CO_2 PSD spectra present the same typical CO $A^1\Pi(v') - X^1\Sigma(v'' = 0)$ vibronic progression as observed for CO. It is therefore assigned to an *indirect* DIET process, driven by CO electronic excitation. From this observation, it is clear that the CO* electronic relaxation transfers some energy to the CO_2 molecules. It is worth noting that this effect appears after pre-irradiation at 8.7 eV, corresponding to only 4% concentration of CO. Significant photodesorption rates, reaching 7×10^{-4} molecules $photon^{-1}$, are observed for an ice film containing about 20% CO (9.8 eV pre-irradiation). At high CO coverage (11 eV pre-irradiation), a decrease in the CO_2 photodesorption rate above 10.5 eV is observed. In this case, the shape of the PSD spectrum is similar to that observed for a pure CO sample, indicating that the desorption is mainly driven by CO molecules. As the energy of the pre-irradiation increases, the CO concentration also increases, and the PSD spectra of CO_2 and CO are in between that of a desorption process dominated by CO_2 excitation and a desorption process dominated by CO excitation. This series of experiments thus simulates how the desorption from an ice sample evolves when continuously irradiated at high photon fluxes.

Discussion

A. Specificities of the energy-resolved and low fluence experimental method

Before discussing the involved desorption mechanisms and photodesorption rates, important specificities of the present experimental conditions need to be pointed out. In this work the direct detection of CO_2 (and CO) molecules in the gas phase is realized by mass spectrometry. This is different from most previous experimental studies, in which the quantitative determination of the CO_2 photodesorption was based on a depletion measurement of CO_2 from the solid phase, either by following solid CO_2 infrared fingerprint spectra during irradiation,[14–16] or by probing the mass loss using a quartz microbalance,[17] but not *via* the gas phase detection of CO_2. In the present study, the analysis of the partial gas phase pressure is assumed to reflect the desorption kinetics from the ice surface, which is generally the case in ultrahigh-vacuum chambers with high pumping speed.[18] In addition, gas phase detection is found to have a much higher sensitivity to surface desorption processes as compared to IR spectroscopy (see also ref. 18). This allows the detailed exploration of desorption mechanisms at low photon fluence that are not accessible by IR spectroscopy. Indeed, the total photon fluence used in PSD never exceeds 5×10^{15} photons cm^{-2} over a complete energy scan, which is about three orders of magnitude lower than in previously reported experiments using H_2 microwave discharge lamps.[14,17,18,25] In this setting, very limited chemistry is induced, as attested by the extremely faint CO IR stretching band observed by RAIRS spectroscopy, together with the non-detection of other chemical species such as CO_3 and O_3, which have been reported in other studies.[14,17] TPD experiments following a PSD spectrum show that the conversion of CO_2 into CO is barely detectable, and doesn't exceed $\sim$0.6% after a PSD scan performed on a fresh CO_2 sample at 10 K. Moreover, it should be pointed out that very little material is removed from the solid phase, since less than 0.04 ML is estimated to be desorbed during a PSD experiment. From these observations, we can conclude that, under the conditions used here, the influence of secondary chemical processes is not favored. For the same reason, the enhancement of desorption rates associated with ice re-structuring can be completely neglected. The data we present here thus focus on the basic molecular processes associated with the initial fast photodesorption of CO_2 and CO species from the outermost surface.

B. Photodesorption mechanisms

Several mechanisms are at play simultaneously in the photodesorption of CO_2 and CO from CO_2 ices. Our experiments, performed on as-grown ices and on pre-irradiated ices, allow us to identify two regimes: (i) photodesorption from as-grown CO_2 samples, consisting of primary processes triggered by the photon absorption of solid CO_2 molecules, and (ii) photodesorption from pre-irradiated films, reflecting *indirect* processes triggered by the photon absorption of solid CO molecules that have been formed and accumulated in the CO_2 ice during pre-irradiation. Fig. 5 gives a summary of the different mechanisms to be considered, which are discussed systematically below.

B1. Desorption from as-grown CO_2 samples. The initial step in the photodesorption is the photon absorption of CO_2 molecules, as illustrated in Fig. 2,

where the energy-dependence of both CO and CO_2 desorption mimics the absorption spectrum of the CO_2 ice. Subsequently, the absorption can lead to dissociation into CO and O. If formed with enough kinetic energy, some of the photofragments can desorb directly after their formation, leading to a CO gas phase signal.

In the case where the photofragments remain trapped within the ice, their recombination–reforming of CO_2, which is exothermic by $\sim$ 5 eV,[53] can also transfer energy to the ice, causing CO_2 to desorb. Indeed, this recombination reaction has a low barrier (40–60 meV) and is known to be active at low temperature ice surfaces.[54] It is interesting to note that H_2O photodesorption is expected to share common properties with CO_2 because of the well-known dissociative character of the first electronic states of H_2O under vacuum UV, producing OH and O photofragments. Indeed, theoretical simulations of H_2O photodesorption in the first absorption band reveal that the exothermic chemical recombination of O atoms and OH fragments contributes to the desorption rates.[55] For CO_2 ice, we estimate the role of this dissociation–recombination process in the overall photodesorption of CO_2. The production of CO_2 by chemical recombination consumes CO molecules. The anti-correlation observed between CO and CO_2 desorption rates when comparing PSD spectra recorded at 10 and 40 K supports this mechanism (Fig. 2). As already mentioned above, this behavior is most probably explained by the dramatic lowering of the surface residence time of CO. At 40 K, the induced thermal CO desorption inhibits chemical recombination, resulting in lower CO_2 desorption rates together with higher CO desorption rates. Assuming that the chemical recombination is completely avoided at 40 K, this effect would contribute to 10% of the total CO_2 photodesorption efficiency.

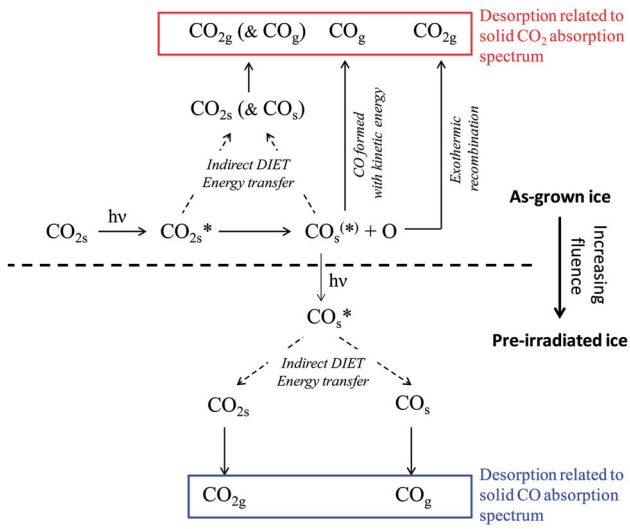

Fig. 5 Scheme of the proposed mechanisms involved in the photodesorption of CO and CO_2 from a CO_2 ice. The primary mechanisms, *i.e.* involving only the absorption of a photon by the CO_2 molecules, are presented in the top part of the figure, whereas the mechanisms requiring a subsequent absorption by the photo-produced CO molecules are shown in the lower part of the scheme.

Consequently, mechanisms other than dissociation–recombination must be at play in the overall CO and CO_2 desorption. This implies that reactive processes have a minor contribution to the overall photodesorption, in agreement with recent conclusions reached by Yuan and Yates.[18]

Theoretical work on water predicts its total photodesorption rate to be largely driven by a "kick-out" mechanism, where fast H atoms produced by photodissociation deeper within the ice travel to the surface and transfer their momentum to a surface molecule.[55] In the case of CO_2 ice, a similar role may be played by O atoms that will carry most of the energy. Taking into account that part of the photon energy is needed for dissociation into specific electronic states, the kinetic energy that is shared between O and CO fragments then increases with the incident photon energy, varying from zero (at the dissociation threshold) up to a few eV above the threshold. Thus, a kick-out mechanism would be observed in our PSD spectra as a continuous increase with increasing photon energy. Such a contribution is not clearly observed.

Beside mechanisms initiated by photodissociation, the DIET process, as previously discussed for N_2 and CO, is associated with the fast relaxation of electronically excited states revealed by strong resonances in the PSD spectra (Fig. 1). It is not possible to extract similar spectral resonances within the continuous desorption above 11 eV for CO_2, which is certainly due to the high density of dissociative states. In this case, due to the lengthening of the C–O bond in the upper repulsive states and subsequent quenching, it has been proposed that highly vibrationally excited molecules are produced within the ice matrix, originating from the Menzel–Gomer–Redhead effect.[56] This energy can be either locally transferred to the surrounding molecules leading to desorption, or dissipated within the ice matrix, depending on the strength of vibrational couplings between the ice components.[15,16] In the case where desorption is induced by energetic VUV photons however, we conclude that excited photofragments also contribute to the desorption process. Excess energy released upon relaxation of CO*, for example formed in its $a^3\Pi$ state with energies between 11 and 14 eV, could be transferred to surrounding CO_2 (or other CO molecules depending on the amount formed), initiating desorption.

Finally, when accurately comparing the PSD spectra to the regular CO_2 absorption spectrum, it should be noted that the sharp peak observed at 10.7 eV in the absorption spectrum is not seen in the PSD spectra. CO_2 dissociation into CO and O fragments therefore is expected to contribute to a direct "CO-from-CO_2" desorption. Because any corresponding CO desorption peak is observed at 10.7 eV, we conclude that this resonance does not induce dissociation. This is certainly linked with the excitonic, and therefore delocalized, character of this resonance, for which the energy is diluted in all the degrees of freedom within the matrix.[36] This energy dissipation may also explain the lack of photodesorption associated with this state.

B2. Desorption from pre-irradiated samples. Our previous investigations have highlighted the importance of indirect desorption in explaining the photodesorption of weakly bound species from a binary ice sample.[29,30] Indirect desorption also plays a role in the photodesorption of CO_2 ice, despite the fact that CO_2 molecules are more strongly bound to the surface. The presence of an indirect desorption mechanism is clearly evidenced by the experiments performed after CO_2 pre-irradiation (Fig. 3), which illustrate that some CO_2 is converted into CO.

In order to interpret these experiments, a comparison with the desorption results from $CO:N_2$ films as previously analyzed is useful (Fig. 1). In the case of binary films, the desorption can be described by a combination (50% each) of pure N_2 and CO desorption rates. Moreover, the desorption is dominated by CO excitation at low energies ($E < 10$ eV), because N_2 absorption is extremely weak below 12 eV. A very similar situation applies to "pre-irradiated" CO_2 samples (Fig. 3), for which low and high energy components can also be attributed to different contributions. In the low energy range, the desorption is dominated by CO excitation because of the low absorption cross section of CO_2. In the higher energy range ($E > 10.5$ eV) the desorption results from a combination of CO_2 and CO excitation. However, a major difference in the $CO:N_2$ case is that the separate weights are not equivalent. This is revealed by considering the ratio between the CO and CO_2 desorption rates. On a pure CO_2 sample, the CO desorption rate exceeds that of CO_2 by a factor of about 2 (Fig. 2). This can be understood by the contribution of CO-from-CO_2 desorption, related to the photodissociation of surface CO_2 molecules. By contrast, the ratio between CO and CO_2 desorption rates increases with increasing CO concentration (Fig. 3). The CO desorption rate exceeds that of CO_2 by one order of magnitude when about half of the CO_2 molecules have been converted into CO (from the experiments after 11 eV pre-irradiation). This huge effect highlights the fact that indirect desorption processes have very different yields for CO and CO_2 molecules. At first sight, this is not very surprising since the CO_2 physisorption energy is about twice that of CO. However, considering the large energy released into the ice film as compared to the binding energies, this suggests differences in the energy transfer efficiency between CO–CO and CO–CO_2 media. This again reinforces the crucial role played by the molecular environment in mediating the energy transfer towards the surface and into a desorption channel, as pointed out previously by Bertin *et al.*[29] and Yuan *et al.*[16]

The weight of the CO excitation-related desorption compared to the CO_2 excitation-related desorption in the total desorption spectra increases with the concentration of photoproduced CO on the surface. As stated previously, this leads to a notable increase in the CO photodesorption, especially in the low energy range, of about an order of magnitude. In addition, it also impacts the CO_2 photodesorption behavior. With increasing CO formation, CO_2 desorption becomes gradually dominated by the CO excitation profile (as can be seen in Fig. 1 for pure CO ice). Interestingly, this has the effect of activating the CO_2 photodesorption in the low energy range (below 10 eV), but also decreases the photodesorption efficiency in the high energy range, since CO-induced desorption is less efficient in this part of the spectrum (Fig. 1).

C. Photodesorption rates

This investigation reveals for the first time a very strong energy dependence of the UV photodesorption rates from CO_2 ice films at very low temperature. The total photodesorption rate from pure CO_2 ices samples between 7 and 14 eV is dominated by energetic photons with an energy above 10.5 eV (Fig. 2). As noted above, this behavior mainly originates from the large difference in the absorption cross section of CO_2 ice below and above 10.5 eV. The maximum desorption rate is 1.6×10^{-3} molecules photon^{-1}, which is much lower than the desorption rates derived by the same method for pure CO or N_2 ices, which peak at 4×10^{-2}

molecules photon^{-1} (Fig. 1). However, a significant enhancement of the CO_2 desorption rate is observed in ices prepared by photolysis due to the additional contribution of photons below 10 eV, resulting in desorption rates as high as 8×10^{-4} molecules photon^{-1}. Such desorption rates are not far from the rates determined by Öberg *et al.*[14] using a hydrogen discharge source, which preferentially emits radiation at around 10.2 eV (Ly-α). It is worth mentioning that our investigation shows that neither CO_2 nor CO significantly photodesorb upon Ly-α excitation. The lamp used is not monochromatic, and although 10.2 eV photons might dominate in experiments using H_2 discharge lamps, "residual" molecular H_2 emission at lower energies can contribute as well, depending on the experimental operating conditions. As mentioned at the beginning of this discussion, a significant quantity of CO molecules is formed at the very beginning of the irradiation, due to the higher fluxes and fluences used in broad band discharge lamp experiments. We thus attribute the CO_2 desorption rates determined previously with hydrogen discharge lamps to indirect desorption induced by the photoproduced CO electronic excitation in the 8–10 eV range. We point out that, even though 10.2 eV photons do not directly induce strong desorption, their role in the surface chemistry should not be neglected in general, as the photoformation of new species can indirectly contribute to the desorption efficiency. It has been shown here that in particular the photons with an energy above 10.5 eV can efficiently convert CO_2 into CO, thus resulting in the enhancement of CO_2 photodesorption by lower energy photons. Hence, it is the cumulative effect of high and low energy photons that leads to effective desorption. Interestingly, a similar interplay between photochemistry and photodesorption at various energies has also been demonstrated in a very recent study by Chen *et al.*[20] on CO photodesorption rates under various operating conditions of an H_2 discharge lamp.

Finally, the relatively moderate desorption rates discussed here should be distinguished from the higher rates ($\sim 10^{-2}$ molecules photon^{-1}) derived for much higher fluences from CO_2 ices at 40–60 K, and for which thermal activation and ice restructuring enhance the desorption. This effect has been extensively described recently and does not contribute to the desorption under these experimental conditions.[17,18]

In the diffuse interstellar medium or at the edge of molecular clouds, highly energetic photons ($E > 10.5$ eV) may contribute to direct CO_2 (and CO) desorption. Deeper inside the molecular clouds, however, the highly energetic component of the spectrum is progressively shielded by gas phase H_2 and CO, which should strongly limit their contribution. However, molecular H_2 emission induced by cosmic rays penetrating into dense clouds produces photons *in situ* (at a lower flux), which are not very efficient in inducing CO_2 desorption. One might conclude that the UV photodesorption of CO_2 is not very efficient in most dense environments compared to other species. However, CO_2 is generally observed in CO_2:H_2O or CO:CO_2 phases.[12] Assuming that the CO:CO_2 component is formed over the H_2O rich layers, the high efficiency of photodesorption driven by CO should therefore contribute to the gas phase enrichment of CO and CO_2 in cold environments. The experiments described above indeed lead to the conclusion that low energy photons ($E < 10.5$ eV) can actually induce the desorption of CO_2 due to indirect desorption, with rates peaking close to 10^{-3} molecules photon^{-1}, despite the fact that pure CO_2 ice is not efficiently photodesorbed in this energy range. In order to further elucidate the relevance of such a process, UV desorption

efficiencies for different concentrations of CO:CO_2 binary mixtures will be needed, which are scheduled for upcoming DESIRS runs using the wavelength-dependent approach described here.

Summary and conclusion

The energy dependence of absolute desorption rates from CO_2 ices have been obtained for the first time using tunable synchrotron radiation between 7–14 eV. The high sensitivity of mass spectrometry enables the quantitative determination of the desorption rates from the direct gas phase detection of CO and CO_2 molecules ejected from the ice. The chosen experimental conditions used in this experiment allow for a systematic comparison of the photodesorption spectra of pure and pre-irradiated CO_2 ices. Hence, the PSD spectra provide a "snapshot" of the different desorption mechanisms at play depending on the UV-processing history of the ice film. In the case of pure CO_2 samples at 10 K, CO_2 and correlated CO desorption are found to proceed mostly above 11 eV, with desorption rates ranging between 1–3 $\times$ 10^{-3} molecules photon^{-1}, whereas no desorption or weak desorption ($<10^{-4}$ molecules photon^{-1}) is observed below 10.5 eV. Chemical recombination, contributing 10% of the total desorption rate at low temperature (10 K), has been identified on the basis of a significant decrease in CO_2 desorption rates at 40 K confirmed by the enhancement of the CO desorption rate, preventing any recombination at the surface of the ice film.

In the case of pre-irradiated samples, the preliminary photolysis of the ice sample dramatically modifies the desorption behavior. A new photodesorption route, due to indirect desorption through CO excitation and fast relaxation is evidenced between 8 and 10 eV, for a concentration of only a few percent of CO within the upper layers of the ice film. This effect is an *indirect* DIET mechanism mediated by high CO absorption cross sections in this energy range. This leads to CO_2 desorption rates up to 10^{-3} molecules photon^{-1}. Although the efficiency of the energy transfer is much lower than that previously observed for the light and weakly bonded species CO and N_2, this mechanism also applies to CO_2. This process may explain the desorption efficiency at higher energies as well.

In conclusion, ice photolysis and photodesorption yields are closely interconnected because the desorption efficiency is very sensitive to the ice composition. Highly energetic VUV photons (10.5–14 eV) are efficient at photodesorbing CO_2 and/or converting CO_2 into CO. Low energetic photons (8–9 eV) are efficient at photodesorbing CO_2 *via* an *indirect* DIET mechanism mediated by CO. This illustrates the complementary role of low and high energy photons in the overall photodesorption efficiency. This interplay is believed to play a major role when induced by polychromatic photon sources, as typically encountered in the interstellar medium, and explains the desorption rates obtained in previous laboratory studies based on broad band discharge lamps, which we attribute mainly to the photoproduction of CO in CO_2 ice.

Acknowledgements

We acknowledge SOLEIL for providing of synchrotron radiation under project 20120834, and we thank Gustavo Garcia for assistance on the beamline DESIRS. Financial support from the French CNRS national program *Physique et Chimie du*

Milieu Interstellaire, the UPMC platform for Astrophysics *"ASTROLAB"*, the Dutch program Nederlandse Onderzoekschool voor Astronomie, and the Hubert Curien Partnership Van Gogh (25055YK) is gratefully acknowledged. The Leiden group acknowledges NWO support through a VICI grant. The authors are grateful to Guillermo Muñoz-Caro and Gustavo Adolfo Cruz-Diaz for sending VUV absorption cross sections prior to publication. J.-H. F. thanks Dr. M. Gudipati for fruitful discussions.

References

1 K. Willacy and W. D. Langer, *Astrophys. J.*, 2000, **544**, 903.
2 C. Dominik, C. Ceccarelli, D. Hollenbach and M. Kaufman, *Astrophys. J. Lett.*, 2005, **635**, L85.
3 D. Hollenbach, M. J. Kaufman, E. A. Bergin and G. J. Melnick, *Astrophys. J.*, 2009, **690**, 1497–1521.
4 V. Guzmán, J. Pety, J. R. Goicoechea, M. Gerin and E. Roueff, *Astron. Astrophys.*, 2011, **534**, A49.
5 A. Oka, A. K. Inoue, T. Nakamoto and M. Honda, *Astrophys. J.*, 2012, **747**, 138.
6 E. Dartois, *Space Sci. Rev.*, 2005, **119**, 293–310.
7 K. M. Pontoppidan, A. C. A. Boogert, H. J. Fraser, E. F. van Dishoeck, G. A. Blake, F. Lahuis, K. I. Öberg, N. J. Evans II and C. Salyk, *Astrophys. J.*, 2008, **678**, 1005.
8 D. C. B. Whittet, P. A. Gerakines, A. G. G. M. Tielens, A. J. Adamson, A. C. A. Boogert, J. E. Chiar, T. de Graauw, P. Ehrenfreund, T. Prusti, W. A. Schutte, B. Vandenbussche and E. F. van Dishoeck, *Astrophys. J. Lett.*, 1998, **498**, L159.
9 A. M. S. Boonman, E. F. van Dishoeck, F. Lahuis, S. D. Doty, C. M. Wright and D. Rosenthal, *Astron. Astrophys.*, 2003, **399**, 1047–1061.
10 N. Sakai, T. Sakai, Y. Aikawa and S. Yamamoto, *Astrophys. J. Lett.*, 2008, **675**, L89.
11 P. Ehrenfreund, A. C. A. Boogert, P. A. Gerakines, D. J. Jansen, W. A. Schutte, A. G. G. M. Tielens and E. F. van Dishoeck, *Astron. Astrophys.*, 1996, **315**, L341–L344.
12 K. M. Pontoppidan, A. C. A. Boogert, H. J. Fraser, E. F. van Dishoeck, G. A. Blake, F. Lahuis, K. I. Öberg, N. J. Evans II and C. Salyk, *Astrophys. J.*, 2008, **678**, 1005–1031.
13 K. M. Pontoppidan, C. P. Dullemond, E. F. van Dishoeck, G. A. Blake, A. C. Boogert, N. J. Evans II, J. E. Kessler-Silacci and F. Lahuis, *Astrophys. J.*, 2005, **622**, 463.
14 K. I. Öberg, E. F. van Dishoeck and H. Linnartz, *Astron. Astrophys.*, 2009, **496**, 281–293.
15 C. Yuan and J. T. Yates Jr, *J. Chem. Phys.*, 2013, **138**, 154302.
16 C. Yuan and J. T. Yates Jr, *J. Chem. Phys.*, 2013, **138**, 154303.
17 D. A. Bahr and R. A. Baragiola, *Astrophys. J.*, 2012, **761**, 36.
18 C. Yuan and J. T. Yates Jr, *Astrophys. J.*, in press, **2014**.
19 T. Kinugawa, A. Yabushita, M. Kawasaki, T. Hama and N. Watanabe, *Phys. Chem. Chem. Phys.*, 2011, **13**, 15785.
20 Y.-J. Chen, A. Chuang, K.-J., G. M. Muñoz Caro, C. Nuevo, M., C.-C. Chu, T.-S. Yih, W.-H. Ip and C.-Y. R. Wu, *ApJ*, 2014, **781**, 15.

21 G. M. Munoz Caro and W. A. Schutte, *Astron. Astrophys.*, 2003, **412**, 121–132.
22 M. S. Westley, R. A. Baragiola, R. E. Johnson and G. A. Baratta, *Planet. Space Sci.*, 1995, **43**, 1311–1315.
23 K. I. Öberg, G. W. Fuchs, Z. Awad, H. J. Fraser, S. Schlemmer, E. F. van Dishoeck and H. Linnartz, *Astrophys. J. Lett.*, 2007, **662**, L23–L26.
24 K. I. Öberg, H. Linnartz, R. Visser and E. F. van Dishoeck, *Astrophys. J.*, 2009, **693**, 1209–1218.
25 G. M. Muñoz Caro, A. Jiménez-Escobar, J. Á. Martín-Gago, C. Rogero, C. Atienza, S. Puertas, J. M. Sobrado and J. Torres-Redondo, *Astron. Astrophys.*, 2010, **522**, A108.
26 L. Nahon, N. de Oliveira, G. A. Garcia, J.-F. Gil, B. Pilette, O. Marcouillé, B. Lagarde and F. Polack, *J. Synchrotron Radiat.*, 2012, **19**, 508–520.
27 E. C. Fayolle, M. Bertin, C. Romanzin, X. Michaut, K. I. Öberg, H. Linnartz and J.-H. Fillion, *Astrophys. J.*, 2011, **739**, L36.
28 E. C. Fayolle, M. Bertin, C. Romanzin, H. A. M Poderoso, L. Philippe, X. Michaut, P. Jeseck, H. Linnartz, K. I. Öberg and J.-H. Fillion, *Astron. Astrophys.*, 2013, **556**, A122.
29 M. Bertin, E. C. Fayolle, C. Romanzin, K. I. Öberg, X. Michaut, A. Moudens, L. Philippe, P. Jeseck, H. Linnartz and J.-H. Fillion, *Phys. Chem. Chem. Phys.*, 2012, **14**, 9929.
30 M. Bertin, E. C. Fayolle, C. Romanzin, H. A. M. Poderoso, X. Michaut, L. Philippe, P. Jeseck, K. I. Öberg, H. Linnartz and J.-H. Fillion, *Astrophys. J.*, 2013, **779**, 120.
31 J. D. Thrower, M. P. Collings, M. R. S. McCoustra, D. J. Burke, W. A. Brown, A. Dawes, P. D. Holtom, P. Kendall, N. J. Mason, F. Jamme, H. J. Fraser, I. P. Clark and A. W. Parker, *J. Vac. Sci. Technol., A*, 2008, **26**, 919.
32 R. S. Freund, R. C. Wetzel and R. J. Shul, *Phys. Rev. A: At., Mol., Opt. Phys.*, 1990, **41**, 5861.
33 K. M. Monahan and W. C. Walker, *J. Chem. Phys.*, 1974, **61**, 3886.
34 N. J. Mason, A. Dawes, P. D. Holtom, R. J. Mukerji, M. P. Davis, B. Sivaraman, R. I. Kaiser, S. V. Hoffmann and D. A. Shaw, *Faraday Discuss.*, 2006, **133**, 311.
35 G. A. Cruz-Diaz, G. M. Munoz Caro, Y.-J. Chen and T.-S. Yih, *Astron. Astrophys.*, 2014, **562**, A119.
36 K. M. Monahan and W. C. Walker, *J. Chem. Phys.*, 1975, **63**, 1676–1681.
37 S. Y. Grebenshchikov, *J. Chem. Phys.*, 2013, **138**, 224106.
38 S. Y. Grebenshchikov, *J. Chem. Phys.*, 2013, **138**, 224107.
39 W. F. Chan, G. Cooper and C. E. Brion, *Chem. Phys.*, 1993, **178**, 401–413.
40 C. Cossart-Magos, M. Jungen and F. Launay, *Mol. Phys.*, 1987, **61**, 1077–1117.
41 M. C. Deschamps, M. Michaud and L. Sanche, *J. Chem. Phys.*, 2003, **119**, 9628.
42 J.-H. Fock, H.-J. Lau and E.-E. Koch, *Chem. Phys.*, 1984, **83**, 377–389.
43 T. G. Slanger and G. Black, *J. Chem. Phys.*, 1978, **68**, 1844.
44 J. A. Schmidt, M. S. Johnson and R. Schinke, *Proc. Natl. Acad. Sci. U. S. A.*, 2013, **110**, 17691–17696.
45 Y. Pan, H. Gao, L. Yang, J. Zhou, C. Y. Ng and W. M. Jackson, *J. Chem. Phys.*, 2011, **135**, 071101.
46 G. M. Lawrence, *J. Chem. Phys.*, 1972, **57**, 5616.
47 G. M. Lawrence, *J. Chem. Phys.*, 1972, **56**, 3435.
48 M. S. Gudipati, *J. Phys. Chem. A*, 1997, **101**, 2003–2009.

49 R. Wagner, F. Schouren and M. S. Gudipati, *J. Phys. Chem. A*, 2000, **104**, 3593–3602.
50 M. J. Loeffler, G. A. Baratta, M. E. Palumbo, G. Strazzulla and R. A. Baragiola, *Astron. Astrophys.*, 2004, **435**, 587.
51 S. A. Sandford and L. J. Allamandola, *Astrophys. J.*, 1990, **355**, 357–372.
52 H.-C. Lu, H.-K. Chen, B.-M. Cheng, Y.-P. Kuo and J. F. Ogilvie, *J. Phys. B: At., Mol. Opt. Phys.*, 2005, **38**, 3693–3704.
53 *CRC Handbook of Chemistry and Physics*, ed. William M. Haynes, CRC Press, 2012.
54 M. Minissale, E. Congiu, G. Manicò, V. Pirronello and F. Dulieu, *Astron. Astrophys.*, 2013, **559**, A49.
55 S. Andersson and E. F. van Dishoeck, *Astron. Astrophys.*, 2008, **491**, 907–916.
56 D. Menzel and R. Gomer, *J. Chem. Phys.*, 1964, **41**, 3311–3328.

